

## The Thermal Wake of Kauai Island: Satellite Observations and Numerical Simulations\*

YANG YANG, SHANG-PING XIE,<sup>+</sup> AND JAN HAFNER

*International Pacific Research Center, SOEST, University of Hawaii at Manoa, Honolulu, Hawaii*

(Manuscript received 12 February 2007, in final form 12 December 2007)

### ABSTRACT

Island thermal effects on the trail cloud band over the central North Pacific are investigated for the lee of Hawaii using satellite observations and a regional atmospheric model. The trail cloud band develops around noon and peaks in cloudiness in the early afternoon. The analysis of numerical simulations of the Kauai wake suggests that a dynamically induced convergence zone forms in the lee of Kauai and Oahu (maximum elevation at 1.5 and 1.2 km, respectively) under the trade wind flow. The island thermal effect significantly modulates the island wake and creates a diurnal cycle of development and decay in the lee cloud band. As solar radiation heats up the island from morning to afternoon, warm air moves downstream (warm advection) from the island in the wake zone, increasing the air temperature, decreasing the air pressure, and enhancing low-level wind convergence in favor of the formation of the trail clouds. Conversely the cold advection during night suppresses cloud formation in the wake. The warm advection and the convergence in the wake increase with the upstream trade wind strength, consistent with satellite observations that the cloudiness increases in the wake under strong wind conditions in the afternoon.

The similarity in the trail cloud and its diurnal cycle between Kauai and Oahu suggests that the thermal wake effect is quite common. The conditions for such a thermal wake are discussed.

### 1. Introduction

Satellite observations frequently reveal interesting cloud patterns in the atmospheric wakes of mountainous islands (Hubert and Krueger 1962; Chopra and Hubert 1965; Chopra 1973; Scorer 1986; Smith et al. 1997; Young and Zawislak 2006). Depending on the large-scale wind and temperature profiles, and the mountain height, these island wakes can take one of many forms including a pair of counterrotating vortices trapped in the immediate lee of the island (Smith and Grubišić 1993), a train of vortices extending far downstream (Young and Zawislak 2006), or a stable wake sometimes topped by cloud trails (Dorman 1994; Nordeen et

al. 2001; Porch and Winiecki 2003; Porch et al. 2006). The strong wind curls in the wake may force ocean circulation changes, triggering active ocean-atmosphere interaction as observed in the long wake of Hawaii (Xie et al. 2001; Hafner and Xie 2003; Sakamoto et al. 2004; Sasaki and Nonaka 2006).

For a uniform flow impinging on an isolated mountainous island, it slows down and may even reverse the direction in the wake, forming a vorticity dipole. In laboratory studies, lee vortices are often attributed to the separation of the viscous boundary layer from the lower surface. In numerical simulations of stratified flow past isolated obstacles, a wake with lee vortices can form without surface friction, with the required vertical vorticity being generated by tilting baroclinically produced horizontal vorticity into the vertical (Smolarkiewicz and Rotunno 1989). Subsequent studies of wake formation have focused on potential vorticity (PV) generation by dissipative processes, such as gravity wave breaking and surface friction (Schär and Smith 1993; Smith 1989; Smolarkiewicz and Rotunno 1989; Schär and Durran 1997; Rotunno et al. 1999). The PV anomalies generated by these processes can be a significant factor in vortex shedding through PV conservation downstream. Weak PV anomalies combined with

\* International Pacific Research Center Publication 509 and School of Ocean and Earth Science and Technology Publication 7274.

<sup>+</sup> Additional affiliation: Department of Meteorology, SOEST, University of Hawaii at Manoa, Honolulu, Hawaii.

*Corresponding author address:* Dr. Yang Yang, National Institute of Water & Atmosphere Research, 301 Evans Bay Parade, Hataitai, Wellington 6021, New Zealand.  
E-mail: yang.yang816@gmail.com

island blocking and surface friction may result in a confluence zone in the wake.

Besides these dynamical effects of orography on airflow, the thermal forcing of islands also affects island-scale circulations, as best manifested in the diurnal cycle over the island of Hawaii (Leopold 1949; Chen and Nash 1994; Yang and Chen 2003; among others). The island thermal effect is especially pronounced in areas with weak surface winds due to island blocking, such as the lee side of the tall and large island of Hawaii. While the thermal forcing over islands has been extensively studied, discussions of the thermal effect on island wakes are few in the literature. In a case study of the lee vortices in Taiwan, Sun and Chern (1993) suggested that the diurnal forcing not only generates land/sea breezes but also controls the vortex shedding and the propagation of vortices. The vortex shedding period becomes shorter as a result of the influence of diurnal forcing. For a stratified flow past an idealized three-dimensional obstacle for nonrotating, inviscid flow with idealized thermal forcing (Reisner and Smolarkiewicz 1994), the characteristic scale of thermal forcing (or the magnitude of trajectory-integrated thermal forcing) at the surface is important to determine if a transition would occur from the blocked flow regime to the unblocked flow regime.

Linear clouds are often observed trailing islands. Dorman (1994) analyzed the Guadalupe Island cloud trail using satellite and radiosonde observations and speculated that it is caused by the mechanical disturbance of the wind field by the island, which raises humidity in the upper part of the inversion-capped marine boundary layer in the wake. Studying satellite images, Nordeen et al. (2001) noted a pronounced diurnal cycle in cloud trails of the tropical western Pacific island of Nauru and showed that they tend to develop around noon and begin to decay in the late afternoon. McFarlane et al. (2005) analyzed surface observations at Nauru and found nighttime low-cloud frequency is much less than the daytime frequency. Matthews et al. (2007) use observations to examine the mesoscale disturbance of the marine atmospheric boundary layer by Nauru. The land surface heating forces the growth of a thermal internal boundary layer, within which a plume of cumulus clouds forms. In a study of the trail clouds of Nauru Island between El Niño and La Niña periods, Porch et al. (2006) suggested that large-scale subsidence at the margins of the convective center of the tropical west Pacific is the major driver in maintaining island cloud trails for distances of hundreds of kilometers. However, the cause of such a diurnal cycle of the trail clouds remains unclear. Since cloudiness tends to peak at dawn over the open ocean, the afternoon peak

of trail clouds is likely to be a result of island thermal forcing, which deserves to be examined thoroughly.

The present study uses satellite observations and a high-resolution numerical simulation to study the diurnal cycle in the wake of Kauai Island over the central North Pacific. Our results reveal the afternoon development of trail clouds lee of Kauai and the neighboring island of Oahu. While the dynamical forcing by island mountains creates favorable conditions (e.g., surface wind convergence) for cloud formation, the island thermal effect overcomes the dynamical forcing and erases trail clouds at night. To emphasize the thermal effect, we call the wake of Kauai with afternoon trail clouds the thermal wake in this paper. A thermal wake is a wake with strong diurnal modulations of clouds and other thermodynamic properties. The terminology does not rule out either the importance of dynamic forcing by island orography or the diurnal modulation of the dynamic forcing. On the contrary, dynamically induced convergence in the wake of Kauai helps the formation of trail clouds during daytime. We will show with numerical simulations that the advection of warm air from the island during the day intensifies the low-level convergence, leading to the formation of a cloud band in the lee.

The rest of the paper is organized as follows. Section 2 introduces the trail clouds lee of Kauai and discusses briefly the dynamical flow regime involved. Section 3 describes the satellite data and the numerical model. Section 4 studies the thermal wake by analyzing both satellite observations and the model simulation, while section 5 contrasts the periods of strong and weak trade winds to corroborate the importance of thermal advection. Section 6 presents wakes lee of Oahu Island and the island of Hawaii based on satellite data analysis. Section 7 is a summary.

## 2. Kauai Island

Kauai Island, with its highest mountaintop at 1500 m MSL and a diameter of roughly 50 km, lies in the northernmost of the Hawaiian island chain, where the east-northeast trade winds prevail most of the year (Schroeder 1993). Under the summer trade wind conditions with the Brunt-Väisälä frequency  $N = 0.008 \text{ s}^{-1}$  and a wind speed of  $U = 8 \text{ m s}^{-1}$ , the Froude number ( $Fr = U/Nh$ ;  $h$  is the height of the barrier) is 0.7 for Kauai Island. According to the linear theory (Smith 1989) and nonlinear numerical studies (Schär and Durran 1997; Bauer et al. 2000) of stratified airflow past an isolated obstacle, Kauai, with  $Fr$  of 0.7 and aspect ratio of 1, falls in the flow regime of gravity wave breaking with wake formation in the lee. A dynamically induced

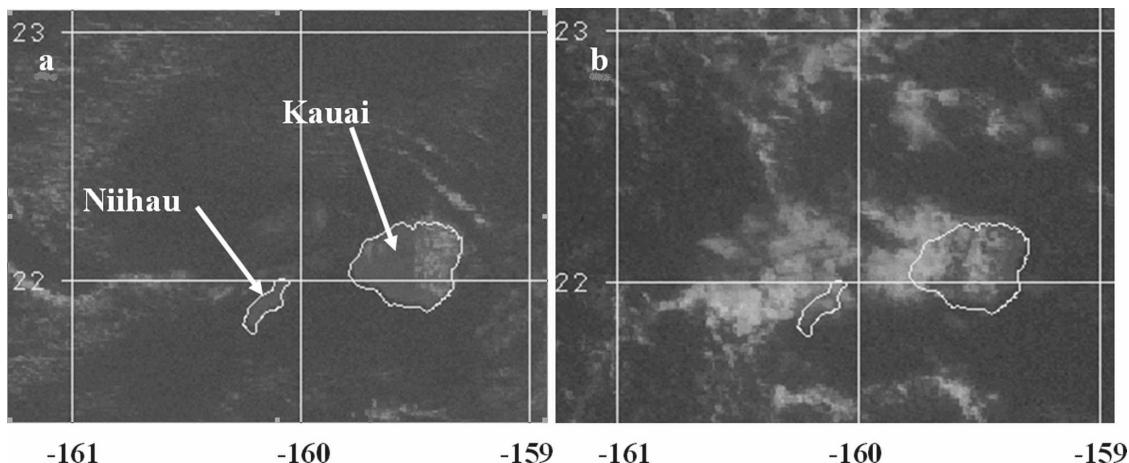


FIG. 1. *GOES-10* visible images at (a) 1030 and (b) 1415 HST 5 September 2006.

return flow and lee vortices are not expected in the wake of Kauai (Smolarkiewicz and Rotunno 1989), unlike the islands of Hawaii and Taiwan (Sun and Chern 1993). Without the return flow in the wake of Kauai, air over the island with diurnal variations in temperature moves downstream and may affect the wake circulations. The dynamical forcing for the Kauai wake has been investigated with numerical simulations by Lane et al. (2006) and Burk et al. (2003), but the island thermal effect on the wake is not considered in these studies.

Figure 1 shows visible cloud images from (Geostationary Operational Environmental Satellite) *GOES-10*. At 1030 Hawaiian Standard Time (HST), no significant clouds were observed over the wake of Kauai Island, but there was a faint and thin cloud trail in the lee of Niihau (Fig. 1a). At 1400 HST (Fig. 1b), the wake was covered by a cloud band that extended 80 km downstream from the west coast of Kauai through Niihau and persisted throughout the whole afternoon. Increased cloudiness over the Kauai wake in the afternoon is very common in the summer, suggesting the importance of diurnal variation of island heating/cooling. Sections 3–5 examine satellite cloudiness climatology over and lee of Kauai through the diurnal cycle and use satellite observations and a numerical simulation to investigate the structure and mechanism for the thermal wake of Kauai.

### 3. Data and model

Polar-orbiting satellites *Terra* and *Aqua* fly over Hawaii about 1100 and 1400 HST during the daytime, respectively. In this study, cloud mask data from the Moderate Resolution Imaging Spectroradiometer

(MODIS) on the *Terra* at 1100 HST and *Aqua* at 1400 HST during June–August of 2004 and 2005 are used to calculate the cloud frequency over the general Hawaii region. Cloud frequency is defined as the total number of days with cloud cover divided by the total number of days considered. For both *Terra* and *Aqua*, only the daytime cloud mask data are used because of the known problems of more clouds than actual over the ocean and false cloud detection over land using infrared data alone during nighttime (additional information is available online at [http://modis-atmos.gsfc.nasa.gov/MOD35\\_L2/qa.html](http://modis-atmos.gsfc.nasa.gov/MOD35_L2/qa.html)). For the daytime cloud mask data, the only known problem is the cloud detection near the coastline. MODIS has a 2330-km-wide swath and a repeat cycle of 16 days, during which one or two swaths do not cover the entire Hawaiian island chain. In this study, we use the swaths covering the entire state.

To illustrate the diurnal cycle better, we use the data from *GOES-10* visible channel 1 (1-km resolution nadir) and IR channel 5 (4-km resolution nadir) with 15-min intervals in August of 2005. Climatologically, the occurrence of the northeasterly trade winds is 92% in August, a month with the most stable and highest frequency of trade wind flow year round. Therefore, August is representative of the entire summer. The radiance from channel 1 is converted to effective albedo, which is smaller over the sea under clear sky than in cloudy conditions. The radiance from the IR channel 5 is converted to brightness temperature. The effective albedo is in a positive relationship with the cloud amount, but this relationship is affected by the diurnal variations of the solar altitude.

We use the fifth-generation Pennsylvania State University–National Center for Atmospheric Research (NCAR) Mesoscale Model (MM5 version 3) (Dudhia

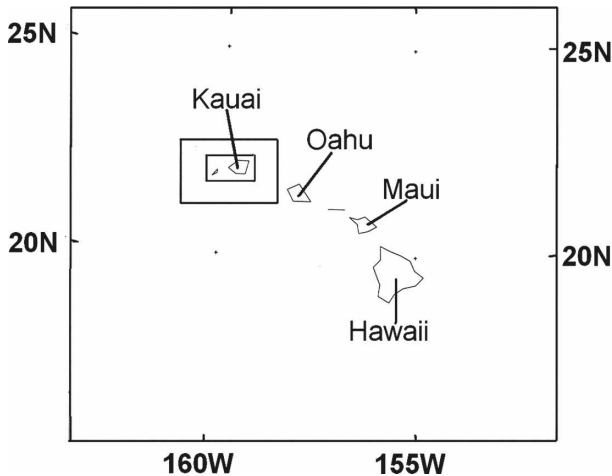


FIG. 2. The three inner nested domains employed in this study with resolution of 9, 3, and 1 km, respectively. The outermost domain is not shown, with 27-km resolution, 120 grids along the east–west direction, and 110 grids along the north–south direction.

1993). It is a nonhydrostatic primitive equation model with the terrain-following sigma vertical coordinate. In this study, there are 34 sigma levels in total<sup>1</sup> from the surface to 100 hPa with 13 of them (0, 8, 24, 47, 71, 95, 119, 159, 239, 442, 734, 1121, and 1455 m) below 1500 m to resolve the boundary layer. Four nested domains with two-way nesting are used with horizontal resolutions of 27, 9, 3, and 1 km (Fig. 2). The Grell cumulus parameterization (employed only for 27- and 9-km resolution domains only), a grid-scale warm rain process (Hsie et al. 1984), a cloud radiation scheme (Dudhia and Moncrieff 1989), and Hong and Pan's (1996) boundary layer scheme are used. An advanced land surface model (LSM) (Chen and Dudhia 2001) is coupled with MM5, with four layers at depths of 10, 40, 100, and 200 cm. The vegetation type, soil type, and vegetation fraction were compiled from the U.S. Geological Survey (USGS) 1:100 000-scale land use/land cover level II data for Hawaii (USGS 1986). The soil types were also compiled from the USGS data with reference to the soil surveys in Hawaii (Foote et al. 1972; Sato et al. 1973), using the procedures described by Zhang et al. (2005) on a 30-in grid. Validating the model against observations during the Hawaiian Rainband Project (HaRP), 11 July–25 August 1990, Yang et al. (2005) show that with the improved land surface

<sup>1</sup> The sigma levels are 1, 0.999, 0.997, 0.994, 0.991, 0.988, 0.985, 0.980, 0.97, 0.945, 0.91, 0.865, 0.82, 0.79, 0.76, 0.73, 0.7, 0.67, 0.64, 0.61, 0.58, 0.55, 0.52, 0.475, 0.425, 0.375, 0.325, 0.275, 0.225, 0.175, 0.125, 0.075, 0.025, and 0.

data of Zhang et al. (2005) the MM5–LSM simulates well the island-scale circulations and their diurnal cycle.

Here we conduct simulations for June–August of 2005 with MM5–LSM, following the procedures of Yang et al. (2005) as described below. The MM5–LSM is spun up for two months, ending 31 May 2005, to obtain appropriate initial soil moisture and soil temperature fields. From 1 June to 31 August, the model is initialized daily at 1200 UTC using the 24-h (h) forecast of the previous day for soil moistures and soil temperatures, and the NOAA Global Forecasting System (GFS)  $1^\circ \times 1^\circ$  analysis for other fields. The GFS analysis is also used for the lateral boundary conditions for the outmost domain. The MM5–LSM is integrated forward for 36 hours. The snapshots are saved every two hours from the 12th to the 36th hour for each daily simulation. A climatologically diurnal cycle is constructed by averaging 92 snapshots from 1 June to 31 August 2005.

#### 4. Thermal wake of Kauai

In this section, we first use MODIS and GOES satellite data to examine the diurnal variations of cloud frequency over the Kauai wake. We then analyze the MM5–LSM simulations to investigate the three-dimensional structure and mechanism of the thermal wake.

##### a. Satellite observations

In the late morning composite (Fig. 3b), larger cloud frequency is found on the windward (with respect to the northeast trades) slopes of Kauai than on the lee side due to orographic lifting of combined trade wind–anabatic flow. On the west edge of the island, cloud cover increases as the sea breeze begins to develop in this region and reduce trade wind speed. The fraction minimum along the north, south, and east coasts is due to the known cloud mask problem on coastlines. From 1100 to 1400 HST (Figs. 3b,c), cloud frequency increases considerably over the leeside land surface of Kauai (by 0.3), Niihau Island, the sea between Kauai and Niihau (0.3–0.4), and the waters downstream of Niihau (0.3–0.5).

The same patterns of cloud cover increase are also found in effective albedo derived from *GOES-10* visible observations (Figs. 4a,b). The mean effective albedo over the sea between Kauai and Niihau and downstream of Niihau is 2%–5% larger in the afternoon than in the morning. The development of trail cloud bands in the afternoon is captured by the distance–time sections of effective albedo along the trade

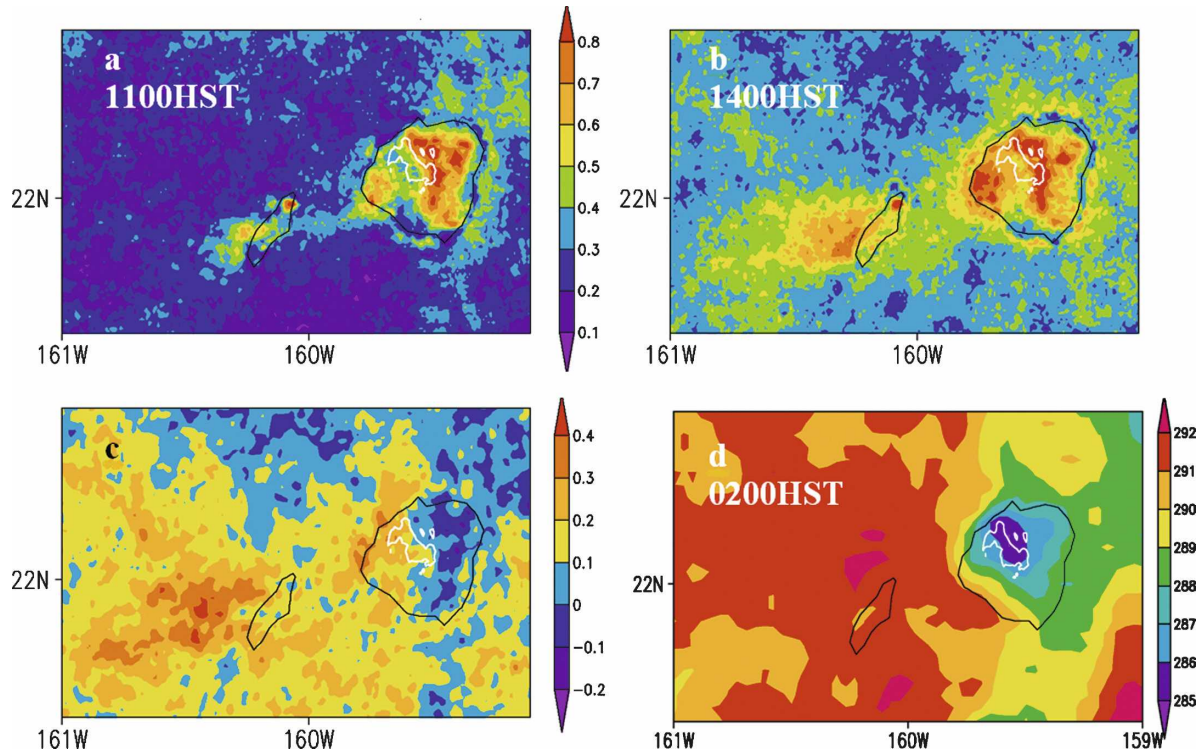


FIG. 3. Cloud frequency for summer 2004 and 2005 at (a) 1100 HST from MODIS *Terra* and (b) 1400 HST from MODIS *Aqua*; (c) the 1400 – 1100 HST difference; and (d) brightness temperature (K) derived from the *GOES-10* IR channel 5 at 0200 HST August 2005. Terrain elevation of 1000 m is shown by the white contour.

wind flow (Fig. 5). Clouds begin to build on the leeside land of Kauai and Niihau from morning and peak in albedo around 1300–1400 HST. Over the leeside sea near Kauai, increased cloud albedo displays a slow downstream propagation at 2–3  $\text{m s}^{-1}$ . Farther downstream 20 km west of Kauai, however, the downstream propagation becomes rather unclear; the cloud albedo increases abruptly from 1200 to 1300 HST, suggesting that the cloud development there is not simply due to the downstream advection of cloud water from the is-

land. MODIS, on the *Aqua* satellite, at 1400 HST captures roughly the peak phase of this lee cloud band. On the leeside area of Niihau (Fig. 5b), the westward propagation of increased cloud albedo is more consistent at about 4  $\text{m s}^{-1}$  within 20 km downstream from the west coast. Farther downstream, the downstream propagation becomes rather unclear. The decay of the lee cloud bands is quite different from the development phase, without any obvious westward propagation, suggesting some nonadvective process at work. The decay

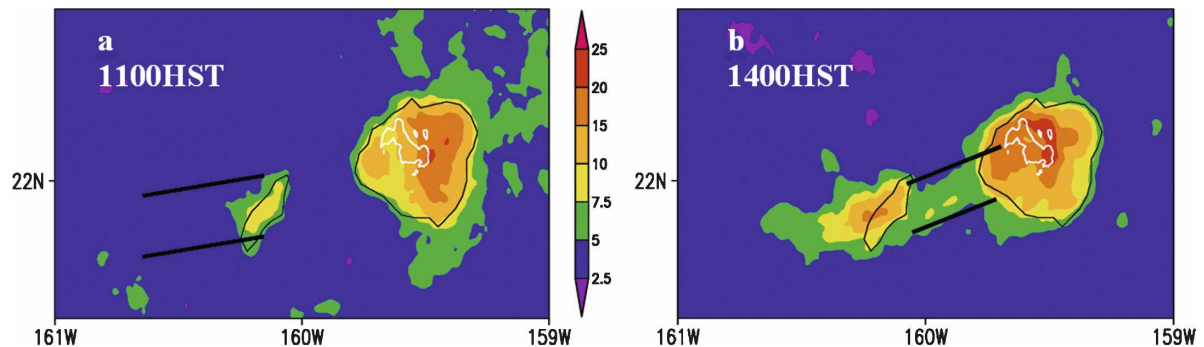


FIG. 4. Effective albedo derived from *GOES-10* visible radiance at (a) 1100 and (b) 1400 HST August 2005. Terrain elevation of 1000 m is shown by the white contour. The solid lines in (a) and (b) outline the area for distance–time section analysis as shown in Fig. 5.

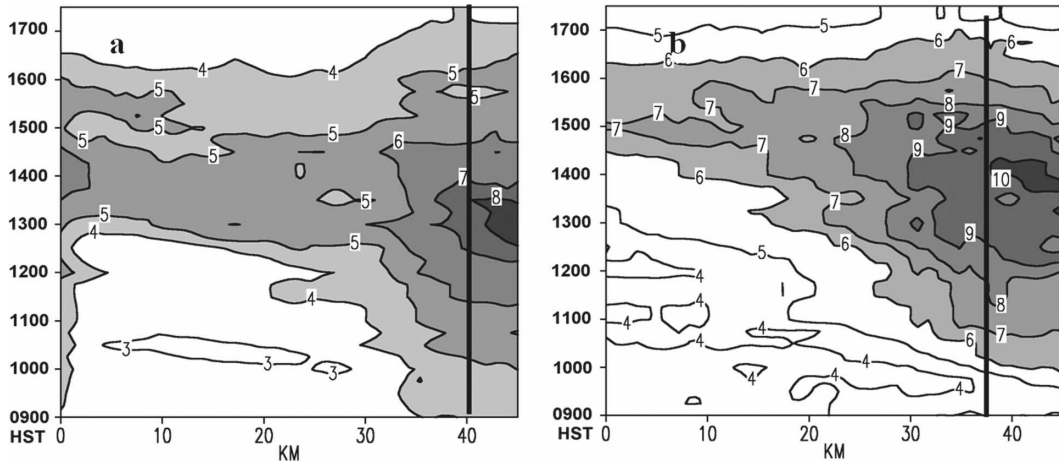


FIG. 5. Along-stream distance–time sections of effective albedo averaged between the thick solid lines in Fig. 4, lee of (a) Kauai and (b) Niihau. The thick straight line marks the island west coast. The 0-km reference point of the  $x$  axis denotes the westernmost point of the area between the two thick straight lines in Fig. 4.

of the cloud band lee of Niihau is particularly rapid, with cloud albedo decreasing from its peak value of 8% to the morning values of 4%–5%.

Over the leeside land surface, continuous land surface heating through morning results in the onset of a weak sea breeze and anabatic flow, which weakens the descent of trade wind flow on the leeside slope. The convergence between the sea breezes/anabatic flow and the trade wind flow leads to increased cloud frequency over the leeside land surface in the afternoon (Fig. 3). Warm air generated over islands and advected downstream by the trade winds may have two competing effects over the nearby sea. One is to increase the low-level air stability as the ocean does not warm much during the day, suppressing convection in the marine boundary layer. Or alternatively, the warm air column may lower surface pressure, inducing horizontal convergence and the rising motion. At night islands cool. The brightness temperature from the *GOES-10* IR channel 4 is 3–4 K higher over the leeside sea than in the upstream environment (Fig. 3d), indicating suppressed cloudiness lee of Kauai and Niihau at night. The afternoon development and nighttime suppression of lee clouds bands as observed by MODIS and GOES support the second scenario.

### b. Numerical simulation

This section tests the above advective thermal wake hypothesis by analyzing the 2-hourly climatology based on the 2005 summer MM5–LSM simulations in the innermost Kauai domain with 1-km resolution. Figure 6 shows the mean simulated vertically integrated cloud water content (ICWC) at 1100, 1400, 0200 HST, and the 1400–1100 HST difference. Larger ICWC is found on

the windward slopes of Kauai because of the orographic lifting of a combined trade wind and anabatic flow. ICWC on the leeside area is persistently less even at 1400 HST, the time when cloud frequency is comparable over land between the windward and lee sides (Fig. 3). This discrepancy suggests that clouds are thicker on the windward side, consistent with the observed larger rainfall amount on the windward slopes than the leeward slopes. On most of the leeside areas, both over land and sea, ICWC at 1400 HST is greater (by 0.01–0.05 mm) than at 1100 HST, consistent with satellite observations (Figs. 3–5).

Kauai is known as one of the wettest places in the world with an annual precipitation of about 11 000 mm (2400 mm for summer) on its highest mountaintop (Giambelluca et al. 1986; Ramage and Schroeder 1999). The simulated rainfall accumulation reaches a maximum of 2200 mm over Kauai on the windward slope close to the mountaintop, with a distribution consistent with observations (not shown).

Over land, rising motions are simulated on the windward slopes of Kauai and Niihau owing to orographic lifting of the trade wind flow while orographic-induced descent is found over the leeside slopes and the northwestern and southwestern leeside areas (Fig. 7b). At 250 m MSL, strong winds ( $10 \text{ m s}^{-1}$ ) are simulated north and south of Kauai as air is forced to flow around the island (Fig. 7a). A wake of weak easterly wind ( $1\text{--}4 \text{ m s}^{-1}$ ) forms lee of Kauai toward which the northeasterly from the north and the easterlies from the south converge. Weak rising motions are found in the wake (Fig. 7b). The dynamically induced convergence zone in the wake favors formation of the trail clouds.

The mean wind patterns in the lee of Kauai (Fig. 7a)

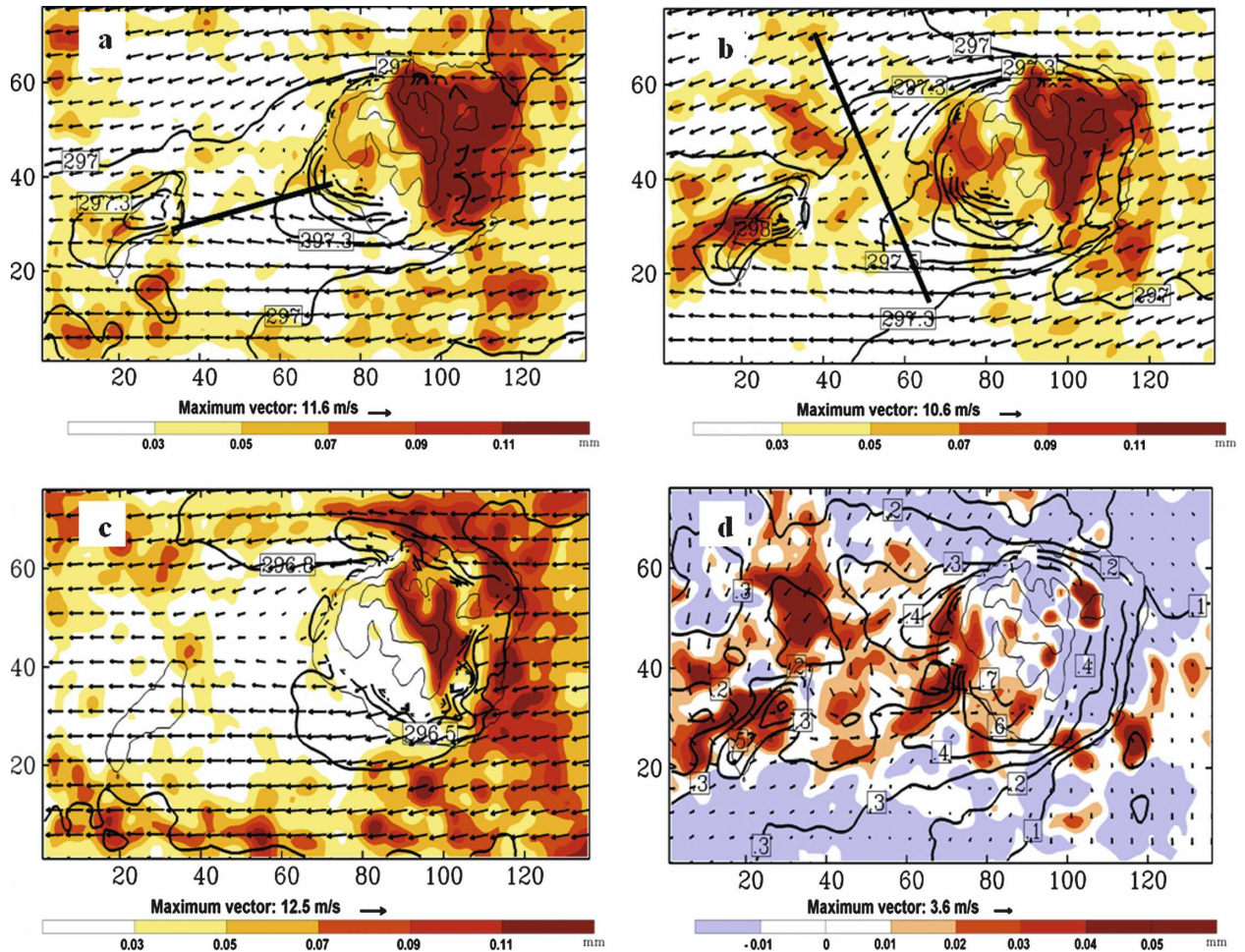


FIG. 6. Simulated wind velocity (vectors in  $\text{m s}^{-1}$ ) and potential temperature (contour intervals at 0.25 K) at 250 m MSL and vertically integrated cloud water content (color shade in mm) at (a) 1100, (b) 1400, and (c) 0200 HST. (d) The 1400 – 1100 HST difference (contour intervals at 0.1 K for potential temperature). The thin solid straight lines show the positions for cross-section analysis. The thick solid straight lines on Kauai are for terrain heights with an interval of 500 m (the same hereafter). Axis labels show grid numbers with grid distance of 1 km.

are comparable to that simulated by Smolarkiewicz and Rotunno (1989) with  $Fr \sim 0.66$ : a flow regime without lee vortices in the wake. We checked individual simulations for each day and found that, for most of the time, lee vortices were not simulated. Occasionally, lee vortices were simulated with a lifetime of 2–4 h, much shorter than those in Taiwan (Sun and Chern 1993) and the island of Hawaii.

Transient lee vortices of Kauai may be due to surface and internal friction in the model. Surface friction can generate vorticity in the boundary layer, which is then carried to the interior of the fluid by boundary layer separation. For a stratified flow past a mountain, surface friction is not required for (e.g., Smolarkiewicz and Rotunno 1989) but may contribute to the lee vortex formation (Ding and Street 2003). In addition, internal

friction and the Reynolds number may also affect lee vortex shedding (Sun and Chern 1994). For example, gravity wave breaking slightly downstream of the mountain crest can generate PV anomalies (Schär and Durran 1997). Further investigations into the transient lee vortex generation are beyond the scope of this paper.

#### 1) DAY AND NIGHT CONTRAST

During the daytime, air temperature is higher in the wake than in the open ocean environment because of the warm advection over the islands and the convergence of the warm air in the wake zone (Figs. 6a,b). With continuous land surface heating from 1100 to 1400 HST, low-level air temperature over the leeside ocean increases by 0.2–0.8 K (Fig. 6d). With the development

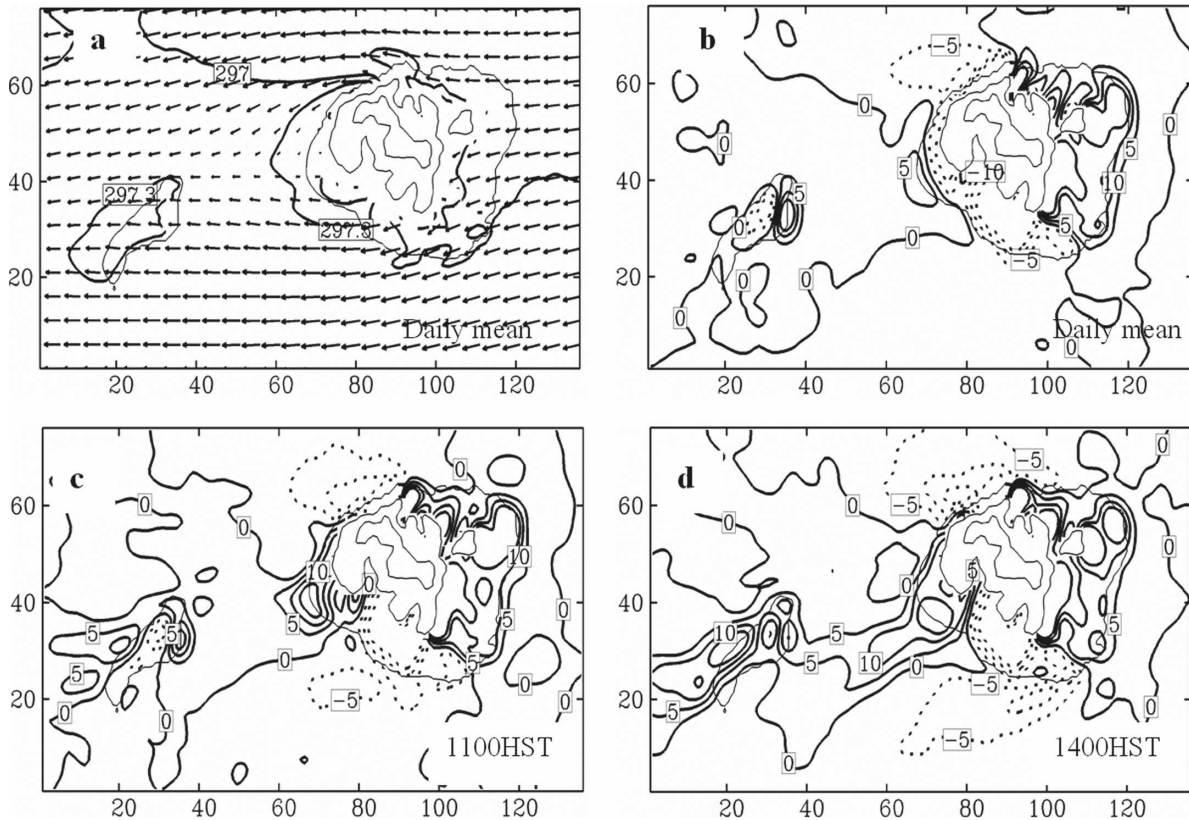


FIG. 7. Daily-mean (a) horizontal wind vectors at 250 m MSL and (b) vertical velocity ( $\text{cm s}^{-1}$ ); mean vertical velocity at (c) 1100 HST and (d) 1400 HST (contour intervals of  $5 \text{ cm s}^{-1}$ ) at 500 m MSL in the summer 2005 simulation. Axis labels show grid numbers with grid distance of 1 km.

of the sea breezes/anabatic flow that further reduces the northeast trades in the wake, warm advection in the wake shifts southward and northward in the afternoon as compared to that in the morning (Figs. 6b,d), with the largest temperature increase on both the northern and southern flanks of the wake. Associated with the warming in the wake, the rising motion over the leeside sea increases in speed to  $5\text{--}10 \text{ cm s}^{-1}$  in the afternoon from  $1\text{--}5 \text{ cm s}^{-1}$  in the morning (Figs. 7c,d).

At night, low-level winds in the wake are easterly and the air temperature is lower than both to the north and south, indicative of the cold advection from Kauai Island (Fig. 6c). ICWC increases over the sea both north and south of Kauai, somewhat consistent with the *GOES-10* IR brightness temperature minima there (Fig. 3d). The ICWC increase is found along the northern and southern boundaries of the model innermost domain, which might be an artifact of compensating rising motions in response to the sinking motions in the wake at night (Fig. 8b).

In the cross-stream section (Fig. 8a) over the sea between Niihau and Kauai, the maximum upward velocity at 1400 HST is found at 1-km level. The upward trans-

port of moist air creates a dome in the equivalent potential temperature field, with clouds forming in the upper marine boundary layer. Compensating downward motions occur on the southern and northern flanks. At night, the anomalous downward motion dominates in the wake, creating a depression in the equivalent potential temperature field with little cloud (Fig. 8b).

In the along-stream cross section, weak sea breezes ( $1 \text{ m s}^{-1}$ ) developed in the afternoon at low levels on the lee coast of Kauai, where rising motion occurs and clouds form (Fig. 9a). On the lee side over the island, the rising motion together with land surface heating results in relatively high equivalent potential temperature from the 500-m to 1500-m level. In this layer, the easterlies prevail, advecting the warm and moist air downstream. [At lower levels, warm advection in the afternoon is found on the northern and southern flanks of the wake where the trade wind flow is strong (Figs. 6a).] At night, equivalent potential temperature is greatly reduced on the lee side of Kauai (Fig. 9b). The easterly trade wind recovers near the surface, facilitating the advection of cool and dry air from the island.

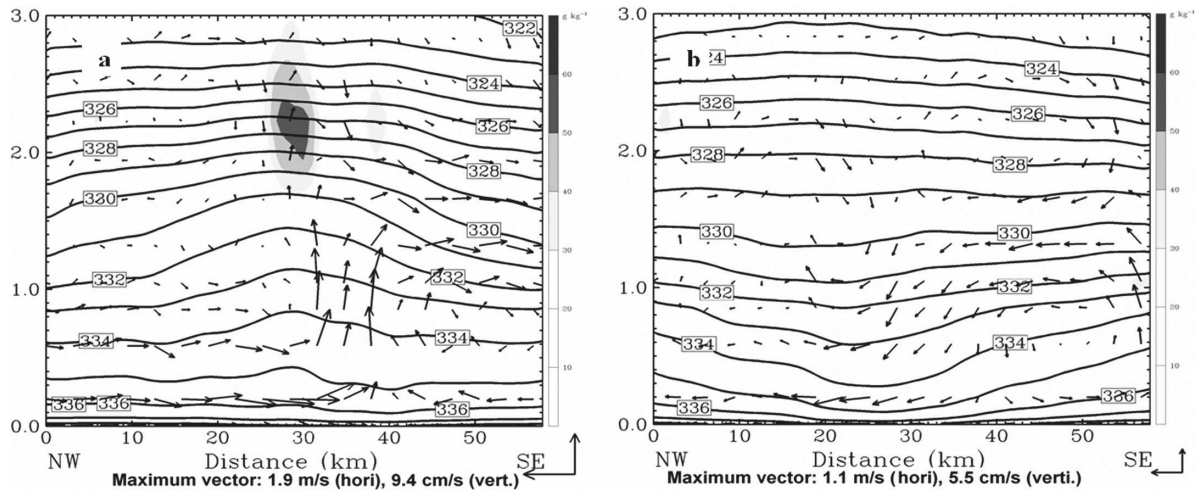


FIG. 8. Cross-stream sections along the line in Fig. 6b of cloud water content (color shade in  $10^{-3} \text{ g kg}^{-1}$ ), equivalent potential temperature (contours in K), and wind velocity at (a) 1400 and (b) 0200 HST. All deviations from the daily mean. The 0-km reference point of the  $x$  axis denotes the northernmost point of the thick solid line in Fig. 6b.

Clouds are few on the leeside coast at night as a down-slope flow (combined katabatic and trade wind flow) develops.

In the following discussion, we isolate the island diurnal heating effect. First, we take the temperature and pressure profiles averaged in a  $50 \text{ km}^2$  area about 30 km to the southeast of Kauai to represent the upstream environmental conditions. Then we subtract temperature and pressure over the leeside sea from the reference environmental profiles, which include planetary-scale tides. Figure 10 shows the cross-stream sections of temperature and pressure anomalies at 1400 and 0200 HST. In the afternoon, positive temperature anomalies with a maximum of 0.4 K, due to the warm advection,

appear at 500 m MSL (Fig. 10a). Near the surface, temperature anomalies decrease because sea surface temperature is kept constant in the model throughout the diurnal cycle. Negative pressure anomalies develop in the marine boundary layer, strengthening toward and reaching the extreme of  $-0.2 \text{ hPa}$  at the surface pressure minimum. The negative pressure anomalies include low-level wind convergence toward the wake. At night (Fig. 10b), the cold advection from the island cools the temperature, with the extreme of  $-0.4 \text{ K}$  at 500 m MSL. Positive pressure deviations develop with a surface maximum of 0.15 hPa. Actually, an increase/decrease in air temperature of 0.3 K for a 1.5-km-deep air column gives a hydrostatic pressure change of 0.18

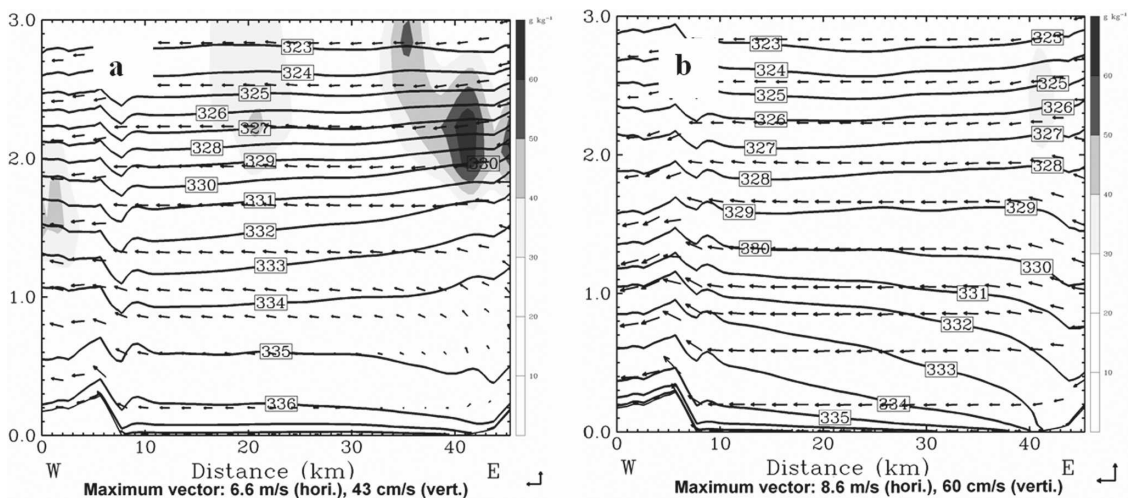


FIG. 9. As in Fig. 8 except for along-stream cross sections along the line in Fig. 6a.

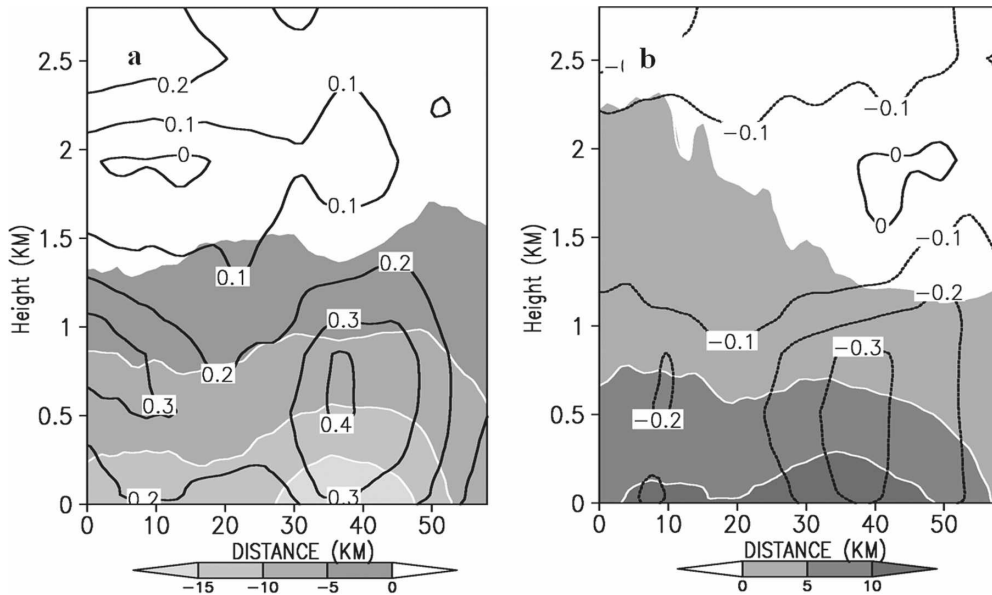


FIG. 10. Cross-stream sections of temperature (black contours in K) and pressure deviations (shade with white contours in hPa) along the line in Fig. 6b from the daily mean at (a) 1400 and (b) 0200 HST. The 0-km reference point of the  $x$  axis denotes the northernmost point of the thick straight line in Fig. 6b.

hPa at the sea surface, roughly consistent with the simulation result.

Recently, a cruise survey was conducted onboard the R/V *Kilo Moana* of University of Hawaii to observe island-induced atmospheric and oceanic circulations lee of Oahu and Kauai Island for 16–20 December 2006 under the trade wind flow. Three soundings were obtained over the sea between Kauai and Niihau Islands at 0630, 1300, and 1700 HST 19 December 2006. At 400 m MSL, the temperature increased by 1.1 K from 0630 HST to 1300 HST, and an additional 0.5 K from 1300 HST to 1700 HST. Continuous shipboard surface air temperature observations revealed a pronounced diurnal cycle in the wake of Kauai Island. These observations are generally consistent with our model simulations.

## 2) FULL DIURNAL CYCLE

Figure 11 displays the full diurnal cycles of vertical velocity, cloud water content, temperature, and pressure at their respective heights of maximum variability. Throughout the diurnal cycle, warmer (colder) air than the open ocean environment is advected downstream from Kauai during the day (at night), causing surface pressure to decrease (increase) and induce low-level wind convergence (divergence) and rising (sinking) motions (Figs. 11a,c). Over the leeside sea off Kauai, the rising motions develop in the morning and peak around 1400 HST with the maximum of  $15 \text{ cm s}^{-1}$  while the

sinking motions peaks around 0500 HST with a maximum of  $-5 \text{ cm s}^{-1}$ . As cloud water in the wake responds to the thermally induced diurnal cycle of vertical motion, more clouds form in the afternoon than at night. Cloud water peaks in the early afternoon in the model (Fig. 11b), in rough agreement with the GOES cloud albedo observations.

## c. Thermal budget

This section uses the simulation data to calculate advection terms in the thermodynamic equation,

$$\frac{\partial \theta}{\partial t} = - \left( u \frac{\partial \theta}{\partial x} + v \frac{\partial \theta}{\partial y} \right) - w \frac{\partial \theta}{\partial z} + \dot{Q}.$$

On the right-hand side are three-dimensional advection of potential temperature and diabatic heating. Over the subtropical ocean, diabatic heating is very small in shallow clouds under trade wind conditions. Figure 12 shows the advection terms in the Kauai wake, averaged vertically from 16 to 1500 m and from 28 to 40 km in the cross-stream distance in Fig. 8. Positive horizontal advection of potential temperature occurs during the day, with negative vertical advection in upward motion. The negative vertical advection peaks at 1400 HST. During night, horizontal (vertical) advection turns negative (positive). The positive vertical advection peaks just before dawn.

The local derivative tracks well the total advection, the latter largely following the horizontal advection.

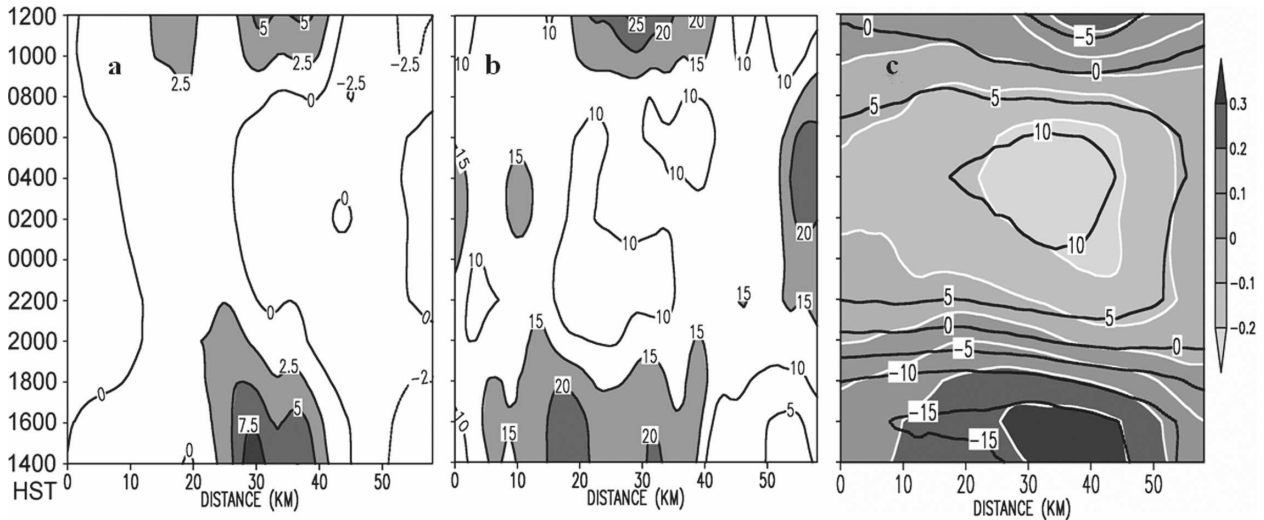


FIG. 11. Diurnal cycles of (a) vertical velocity ( $\text{cm s}^{-1}$ ) at 500 m, (b) cloud water content ( $\text{g kg}^{-1}$ ) at 2200 m, and (c) temperature at 500 m (shade with white contours in K) and surface pressure (black contours in Pa) along the solid line in Fig. 6b. All deviations from the daily mean with the environmental values subtracted. The 0-km reference point of the  $x$  axis denotes the northernmost point of the thick straight lines in Fig. 6b.

There are some small differences between the local derivative and total advection. Possible sources of these differences are diabatic heating and sensible heat flux from the sea surface. Surface sensible heat flux is a weak damping for the diurnal cycle in boundary layer temperature, an order of magnitude smaller than the horizontal advection (not shown).

These results indicate that the warm advection during the day increases the air temperature in the wake, inducing a thermal direct circulation in the cross-stream direction with trail clouds forming in the ascending branch. At night, the whole process reverses. The vertical circulation in Fig. 8 is typical of the atmospheric response to thermal forcing in the boundary layer.

### 5. Sensitivity to trade wind strength

This section investigates how trade wind strength affects the wake of Kauai with satellite observations and model simulations. Wind speed and direction data on 1000 and 925 hPa at four grid points about 100–200 km upstream of the island chain from the GFS  $1^\circ \times 1^\circ$  analysis at 1400 HST are used to classify strong and weak trade wind days in the summers of 2004 and 2005. A strong (weak) trade wind day is chosen when the wind speed is larger (smaller) than  $8.5 \text{ m s}^{-1}$  ( $6.5 \text{ m s}^{-1}$ ) with a direction between  $70^\circ$  and  $90^\circ$  from north. With these criteria, 16 and 15 strong trade wind days are chosen in 2005 and 2004, respectively while there are 16 and 14 weak trade wind days in 2005 and 2004, respectively. We use these classifications for the analysis of

model output during the summer of 2005. The low-level winds upstream of the Hawaiian island chain from GFS data are  $9.5 \text{ m s}^{-1}$  for the strong and  $5.5 \text{ m s}^{-1}$  for the weak trade wind days, with a nearly easterly direction for both composite groups (Fig. 13).

#### a. Satellite observations

The trade wind inversion height is an important factor for cloud cover over Hawaii and nearby waters (not shown). For MODIS cloud frequency composites, we

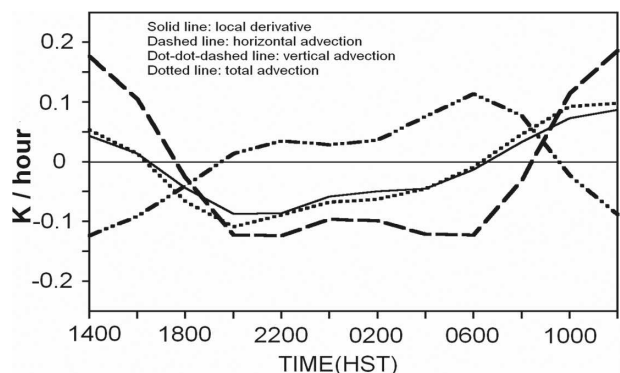


FIG. 12. Diurnal variations of terms ( $\text{K h}^{-1}$ ) in the potential temperature equation in the Kauai wake: local derivative (solid line), horizontal (dashed), vertical (dot-dot-dashed), and total advection (dotted). All terms have been averaged between 16 and 1500 m in the vertical, between 28 and 40 km in cross-stream distance (Fig. 8), and between 5 km east of the easternmost point of Niihau and 5 km west of the westernmost point of Kauai in the along-stream direction.

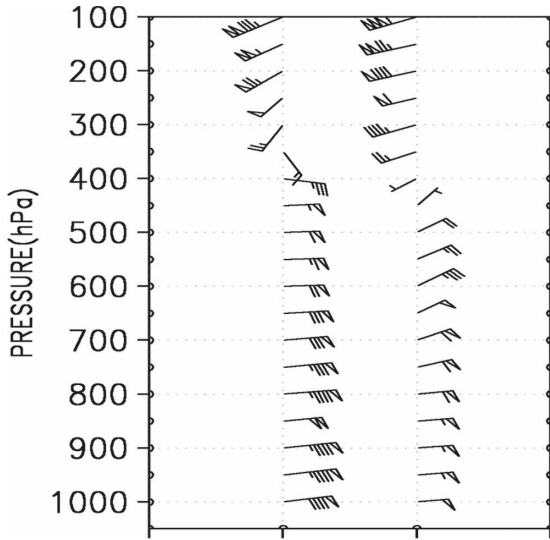


FIG. 13. Wind profiles averaged for strong (left) and weak (right) trade wind days from the GFS analysis 200–300 km upstream of Hawaii during the summers 2004 and 2005. Pennants, full barbs, and half barbs represent 5, 1, and 0.5 m s<sup>-1</sup>, respectively.

require that the inversion height falls between 1600 and 2550 m in the soundings of Lihue, Kauai, to minimize the effect of inversion height variability, in addition to the requirement that MODIS *Aqua* swaths cover the entire state. These criteria give 10 strong trade wind days in 2005 and 9 in 2004, and 9 weak trade wind days in 2005 and 9 in 2004.

Figure 14 shows the MODIS *Aqua* cloud frequency at 1400 HST for the strong and weak wind composites. On the windward slopes of Kauai, the cloud frequency for the strong trade wind days is greater than for the weak trade wind days, typically by 0.2–0.5 in response to the intensified trades and increased orographic lifting. On the western half of the island, cloud frequency decreases slightly for the strong trade wind days because of the stronger descent in the lee of the mountains and a reduced sea breeze–anabatic flow. For the strong trade wind days, cloud cover increases by 0.2–0.3 in the sea channel between Kauai and Niihau and by 0.3–0.5 over the waters lee of Niihau, possibly a result of increased warm advection from islands inducing stronger low-level wind convergence as shown in the following analysis of model simulations. Besides changes in island influences, cloud cover increases by

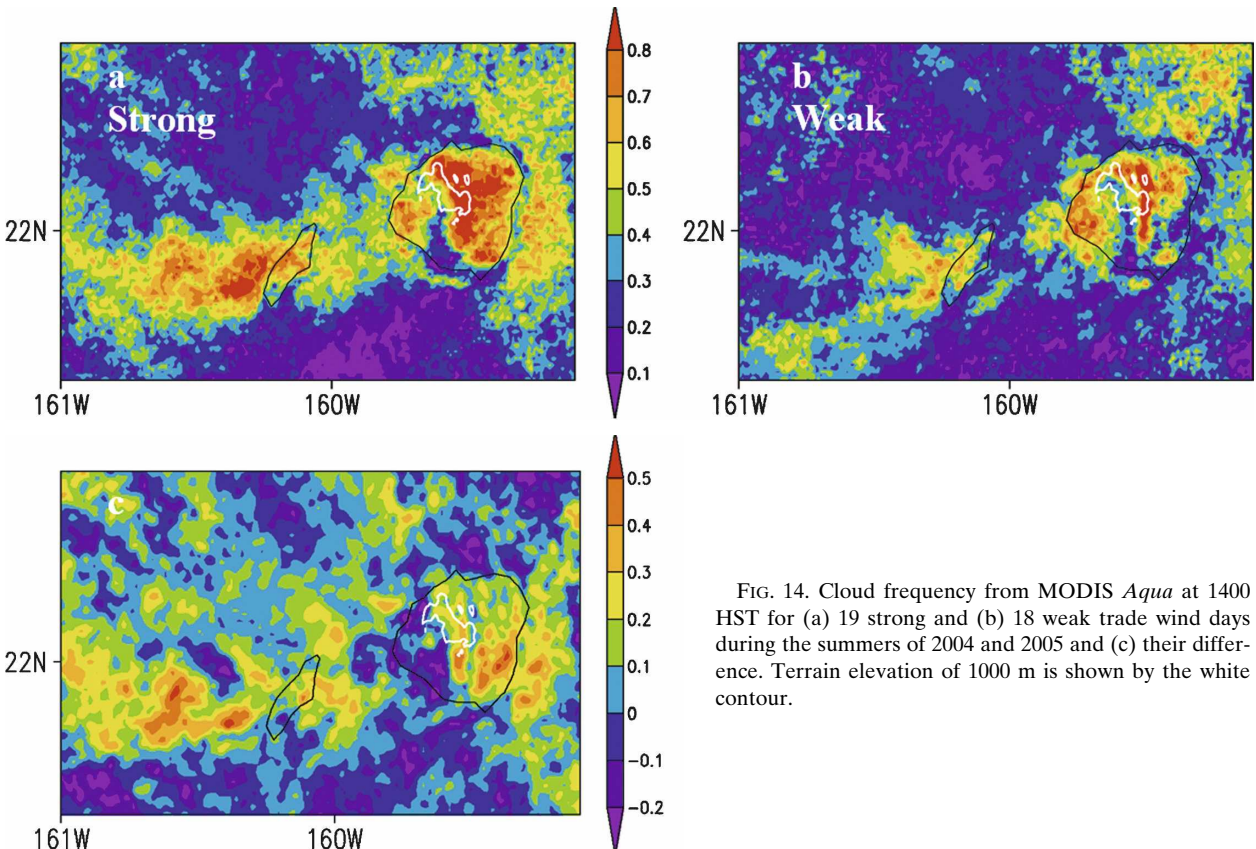


FIG. 14. Cloud frequency from MODIS *Aqua* at 1400 HST for (a) 19 strong and (b) 18 weak trade wind days during the summers of 2004 and 2005 and (c) their difference. Terrain elevation of 1000 m is shown by the white contour.

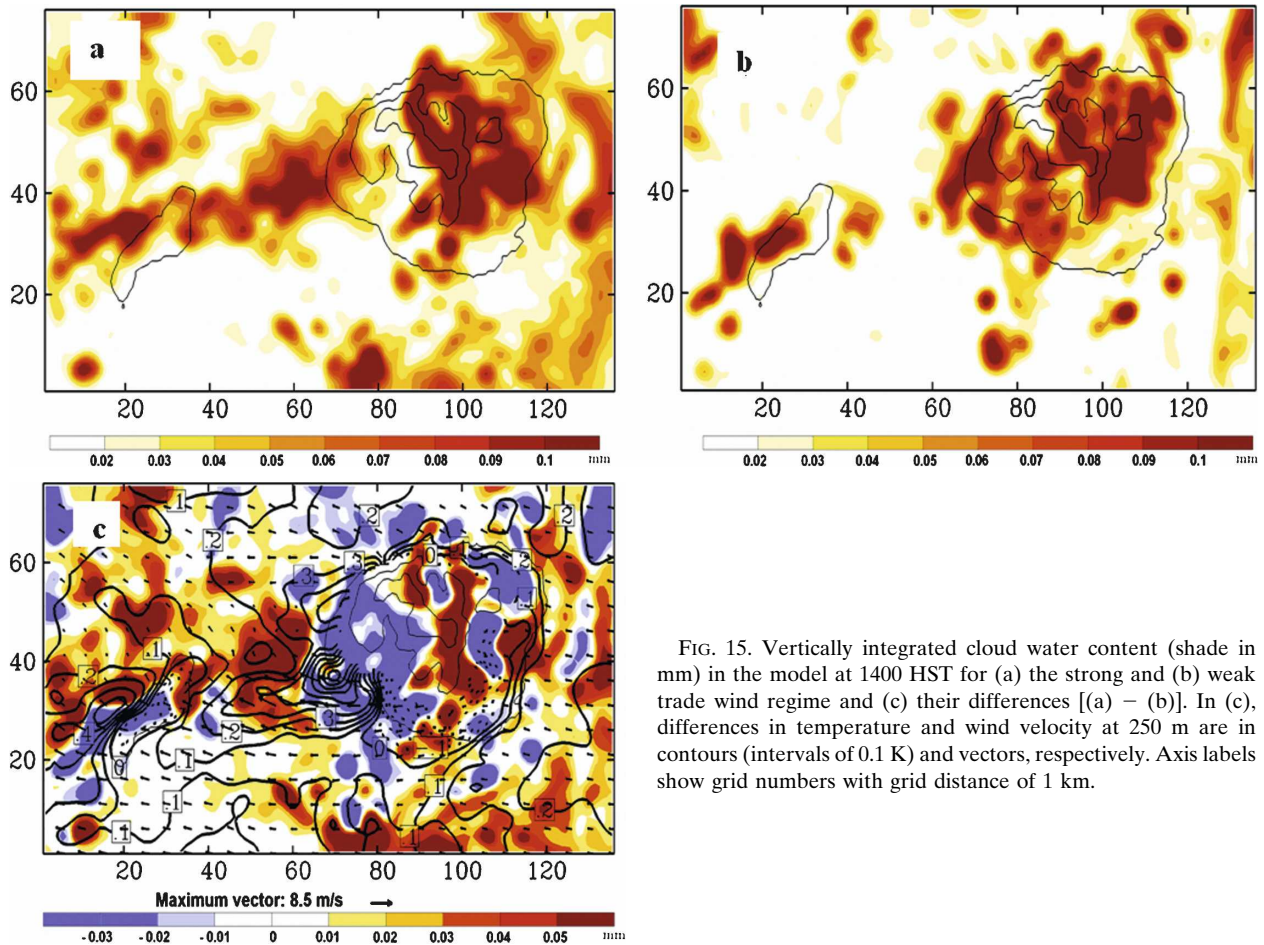


FIG. 15. Vertically integrated cloud water content (shade in mm) in the model at 1400 HST for (a) the strong and (b) weak trade wind regime and (c) their differences [(a) - (b)]. In (c), differences in temperature and wind velocity at 250 m are in contours (intervals of 0.1 K) and vectors, respectively. Axis labels show grid numbers with grid distance of 1 km.

0.1–0.2 over the open ocean environment in response to the increased wind speed.

### b. Numerical simulation

Figure 15 shows the simulated ICWC for the 16 strong and 16 weak trade wind flows during the summer of 2005 and their difference at 1400 HST. There is a general tendency that ICWC increases on the windward half and decreases on the leeward half of Kauai in the strong wind composite in response to stronger orographic lifting and descent, respectively. ICWC increases also in the sea channel lee of Kauai: a well-defined linear cloud band forms lee of Kauai and Niihau in the strong wind but not in the weak wind composite. These results are broadly in agreement with MODIS *Aqua* observations. Considerable increases of 0.2–0.4 K in 250-m temperature in the Kauai wake hint at the intensified warm advection from Kauai as the cause of the organized cloud line in the strong wind composite.

For Kauai Island,  $Fr$  is 0.8 for the strong and 0.5 for the weak trades. Because Kauai Island is roughly cir-

cular and the low-level wind direction upstream is almost the same for both strong and weak trades, a wake circulation is expected for Kauai Island according to Smolarkiewicz and Rotunno (1989). For the weak trades with  $Fr \sim 0.5$ , the leeside circulations are approaching the low Froude number ( $Fr < 0.5$ ) flow regime with lee vortices. Actually, lee vortices with lifetime of 2–4 h were simulated sometimes. The occurrence of lee vortex is more frequent for the weak trades than for the strong trades. The mean wind patterns for the strong and weak trades are, however, quite similar with reduced easterly winds in the wake zone (Figs. 16a,b). Similar to the mean state during the summer, a dynamically induced convergence zone with weak rising motions forms in the lee of Kauai for both the strong and weak trades (Figs. 16e,f). The main differences are the simulated easterly winds, and the dynamically induced rising motions in the wake are stronger for the strong trades than for the weak trades (Figs. 16e,f). These simulations suggest that the wake circulations of Kauai under the strong and weak trades are roughly in the same flow regime with wake formation.

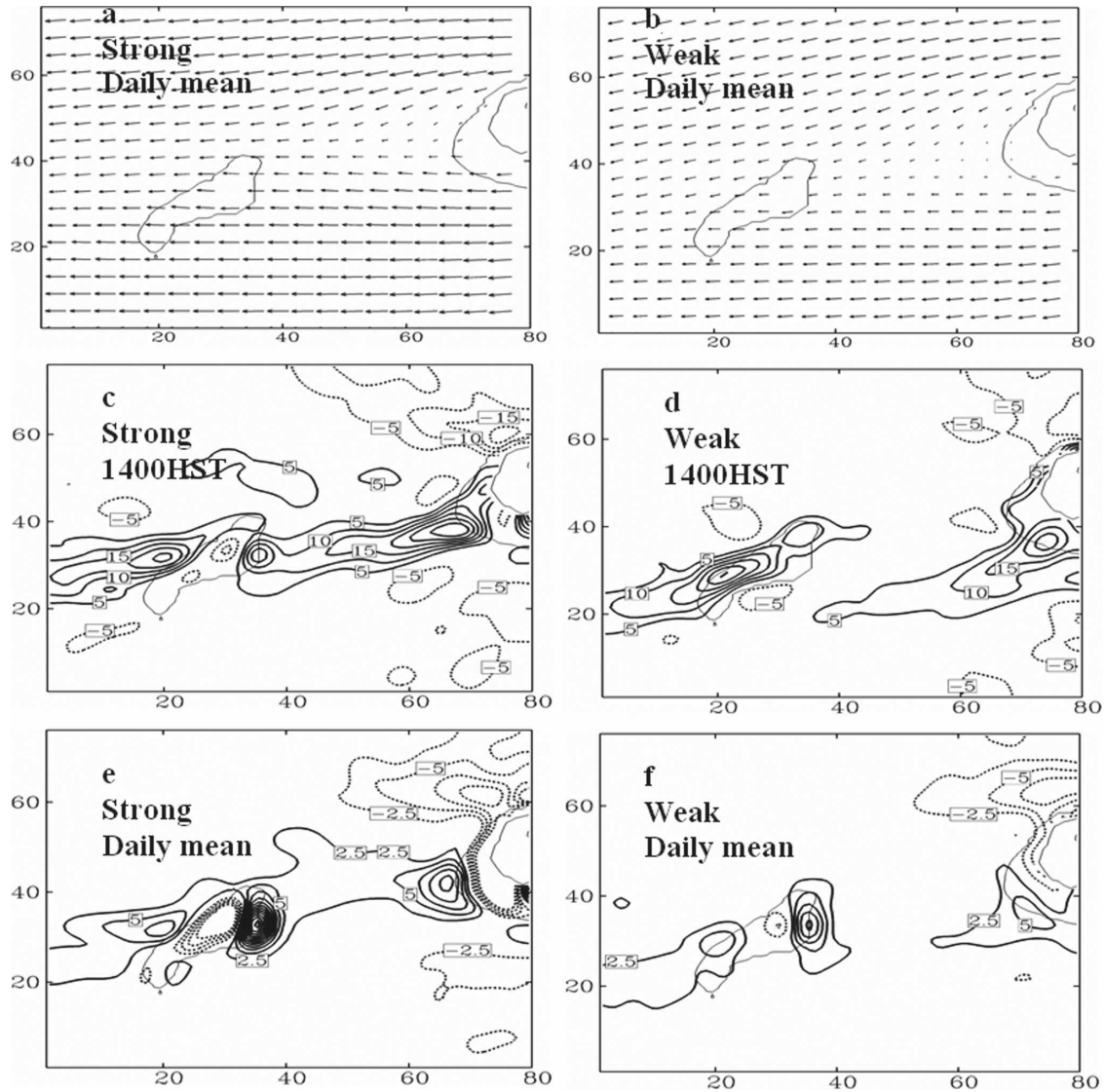


FIG. 16. Daily-mean winds at 250 m above the sea level for (a) the strong and (b) the weak wind regime during the summer 2005. Maximum wind vector is  $12.5 \text{ m s}^{-1}$ . Vertical velocity ( $\text{cm s}^{-1}$ ) at 500 m MSL at 1400 HST for the (c) strong and (d) weak wind regime; daily mean for the (e) strong and (f) weak wind regime; axis labels show grid numbers with grid distance of 1 km.

Figure 16 contrasts vertical velocity at 500 m between the strong and weak trade wind days during the 2005 summer at 1400 HST (Figs. 16c,d). In the strong wind composite, a band of upward motion develops at 1400 HST between Kauai and Niihau and lee of Niihau, consistent with satellite observations and simulations of cloud. In the weak wind map, the upward motion band lee of Kauai shifts slightly to the south. Besides this shift in position, upward motion is considerably stronger under strong wind conditions, by  $5\text{--}10 \text{ cm s}^{-1}$  along the axes of the cloud bands. This enhanced vertical motion may be due to the increased warm advection from Kauai and/or the increased dynamical forcing by

island mountains. To test the hypothesis, we contrast the daily-mean vertical velocity between the strong and weak wind days (Figs. 16c,d). The daily mean filters out the diurnal cycle and may be taken as a measure of dynamical orographic effects. Indeed, the daily-mean vertical velocity increases under the stronger trades, both over islands and nearby waters. The difference of the daily-mean vertical velocity between strong and weak trades, which measuring the dynamical effect, is far smaller than the 1400 HST difference. For example, in the middle of the sea between Kauai and Niihau with grid number of 50, the former difference is  $2.5 \text{ cm s}^{-1}$  while the latter  $7.5 \text{ cm s}^{-1}$ , leading to a rough estimate

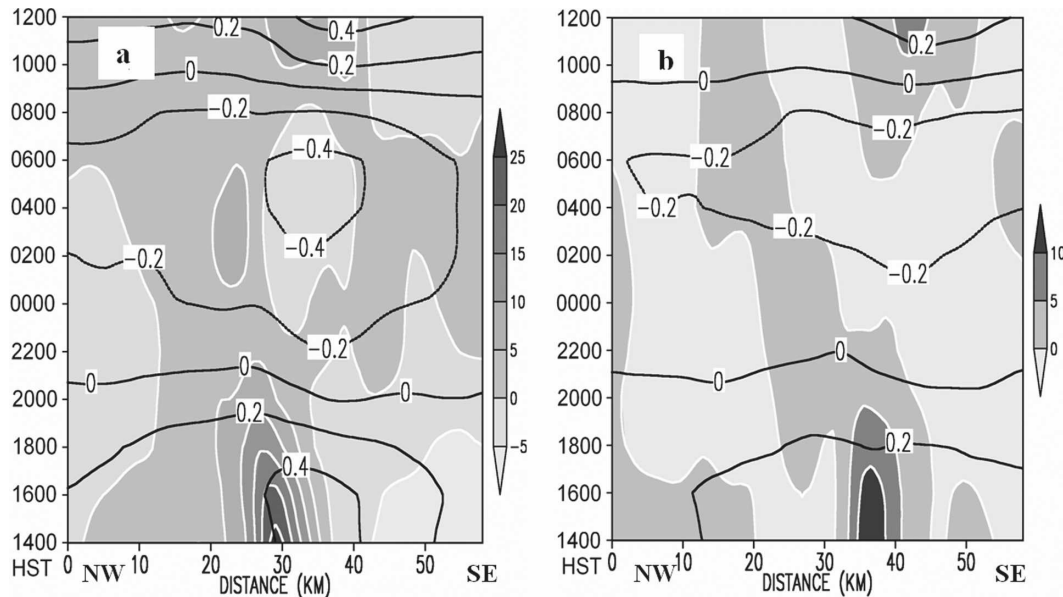


FIG. 17. Cross-stream distance–time sections along the line in Fig. 6b of temperature and vertical velocity (shade in white contours in  $\text{cm s}^{-1}$ ) at 500 m MSL for the (a) strong and (b) weak trade wind regime. The 0-km reference point of the  $x$  axis denotes the northernmost point of the thick straight lines in Fig. 6b.

of the dynamical-to-thermal forcing ratio of 1:2. Indeed, the cross-stream distance–time sections show that the diurnal temperature anomalies increase by a factor of 2 from the weak-to-strong trade wind composite (Fig. 17), suggesting that the enhanced thermal advection, together with the increased dynamical forcing, induces stronger vertical motion.

## 6. Wakes of Oahu and Hawaii

A pronounced diurnal cycle is also detected in the trail cloud band lee of Oahu Island, southeast of Kauai. With a width of 45 km and a length of 60 km, Oahu features two mountain ridges with a north-northwest–south-southeast orientation: the Koolau Range on the east half of the island with a maximum elevation of 1200 m, and the Waianae Range on the western side with a maximum elevation of 800 m. Under the summer trade wind conditions with  $N = 0.008 \text{ s}^{-1}$  and mean wind speed  $8 \text{ m s}^{-1}$ , the Froude number is 0.9. The aspect ratio of Oahu Island is 1.3. According to numerical studies of nonlinear flow by Bauer et al. (2000), the trade wind flow past Oahu is in the regime of mountain-wave breaking with wake formation.

Figure 18 shows the mean cloud frequency from MODIS *Terra* and *Aqua* for 2004–05 summers. In the late morning, clouds mainly occur over the island and the leeside coastal ocean with a maximum along the Koolau Range. In the afternoon, a cloud band develops

also over the ocean lee of Oahu, extending for nearly 100 km (Fig. 18a). The cloud frequency difference between 1400 and 1100 HST over the lee cloud band is 20%–40%.

The afternoon development of the trail cloud band is further confirmed by effective albedo observations from the *GOES-10* visible channel (Fig. 19). In the afternoon, the effective albedo over the leeside sea of Oahu is 2%–5% higher than in the late morning (Figs. 19a,b). The cloud albedo in the wake of Oahu reaches a maximum in the early afternoon in the along-stream distance–time section (Fig. 19d). Clouds on the leeward part of Oahu Island develop in the early morning, much earlier than over Kauai or Niihau Island (cf. Fig. 5). The steady development of the wake clouds does not begin until late afternoon, and the albedo = 5% contour does not show a clear westward phase propagation, suggesting that it is not simply due to the advection of clouds formed on the island. (There is, however, some westward propagation in cloud albedo overall.) At night, brightness temperature is higher in the wake than in surrounding waters (Fig. 19c), indicating suppressed cloud formation there. All this indicates that the diurnal cycle of the wake cloud band lee of Oahu is similar to that lee of Kauai and suggests that the same mechanism of the thermal advection is at work.

For the island of Hawaii with maximum elevation 4200 m ( $Fr \sim 0.2$  under the trade wind conditions), the wake circulations are characterized by two lee vortices

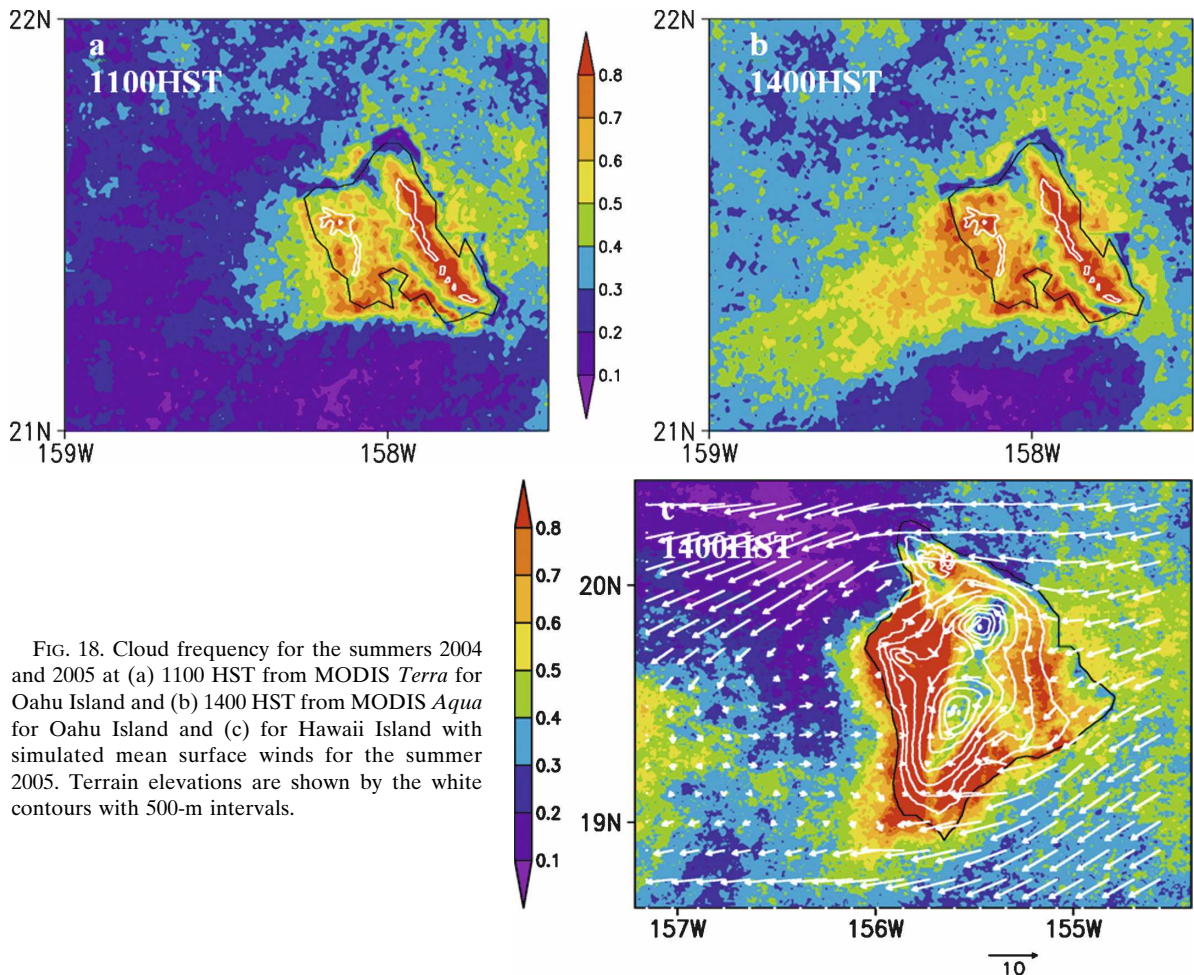


FIG. 18. Cloud frequency for the summers 2004 and 2005 at (a) 1100 HST from MODIS *Terra* for Oahu Island and (b) 1400 HST from MODIS *Aqua* for Oahu Island and (c) for Hawaii Island with simulated mean surface winds for the summer 2005. Terrain elevations are shown by the white contours with 500-m intervals.

and a westerly reverse flow (Smith and Grubišić 1993; Yang and Chen 2003). Figure 18c shows the simulated daily-mean surface winds and MODIS cloud frequency at 1400 HST for summer 2005. On the lee side, maximum cloud frequency is found on the slopes owing to the sea/mountain breeze. High cloud frequency extends slightly offshore west of the Kona coast. In the wake, the strong orographic forcing induces a westerly reverse flow that is 1800 m deep (Yang and Chen 2008) and extends for 150 km downstream. During the day, the sea breeze accelerates the westerly reverse flow, preventing warm air from being advected into the wake from the island at low levels. Indeed, the wake of the island of Hawaii during the day is colder than the northwestern and southwestern leeward areas, inducing a low-level divergence in the wake (not shown). As a result, cloud frequency is small in the cold wake of Hawaii in the afternoon, in contrast to large cloud occurrence in the warm wakes of Kauai and Oahu. Thus flow regime and thermal advection strongly affect the cloud formation in the wake.

## 7. Summary

We have used satellite observations and numerical simulations to study the formation of cloud lines that often trail islands. From MODIS *Terra* and *Aqua* and *GOES-10*, we detect a pronounced diurnal cycle in cloud frequency/albedo trailing islands of Kauai/Niihau and Oahu for as far as 100 km. These lee cloud bands develop around noon, peak in cloudiness in early afternoon, and decay in late afternoon. At night, brightness temperature reaches a local maximum in the wake seen in satellite infrared observations, indicative of suppressed cloud development. Although cloud lines commonly observed lee of islands are often attributed to the dynamically induced low-level wind convergence in the wake, our numerical results show that island thermal forcing can modulate the dynamically induced convergence, creating a diurnal cycle of development and decay in the lee cloud band.

Results from MM5-LSM simulations of the Kauai wake suggest the following thermal wake mechanism.

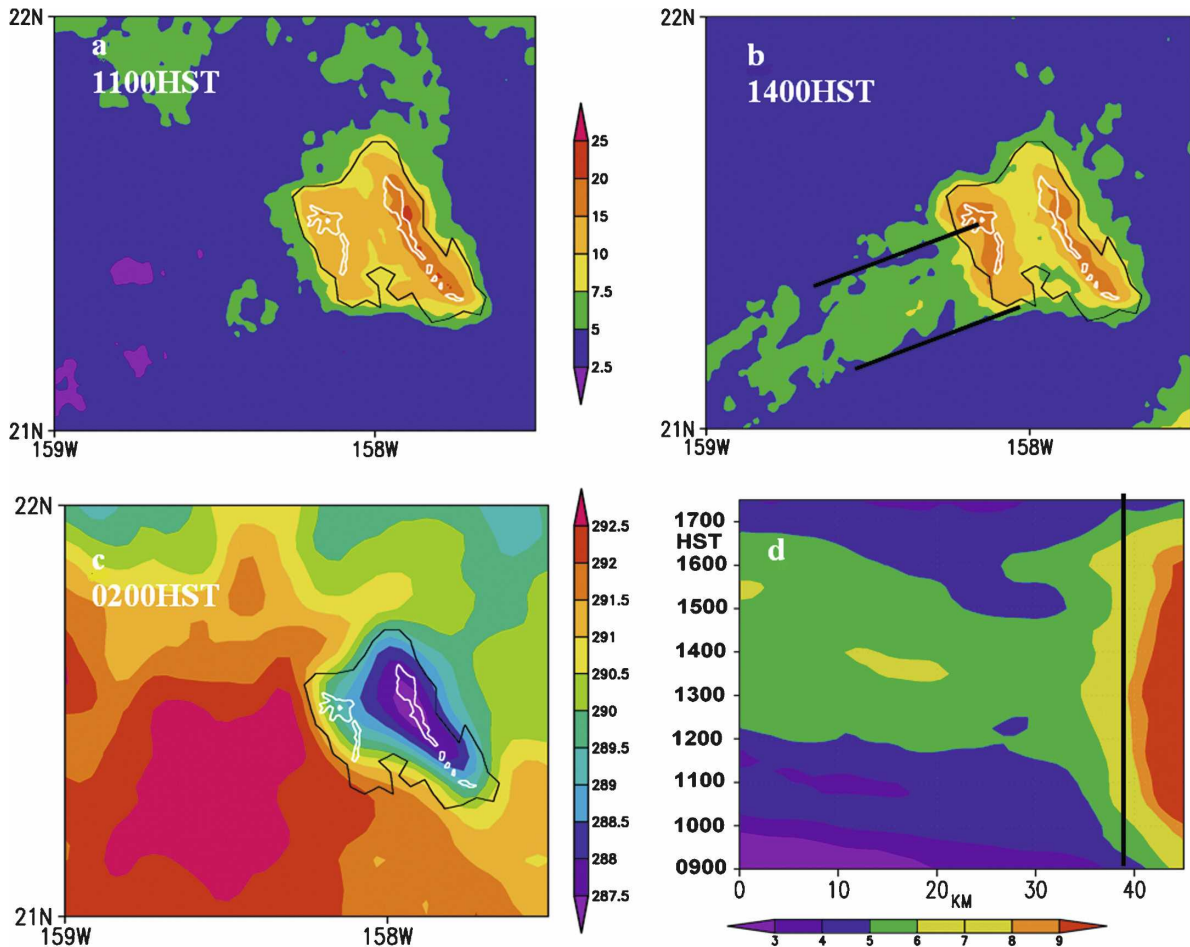


FIG. 19. Effective albedo derived from *GOES-10* visible radiance at (a) 1100 and (b) 1400 HST August 2005. (c) Mean temperature (K) derived from *GOES-10* IR radiance at 0200 HST. (d) Along-stream distance–time section of effective albedo averaged between the two thick straight lines in (b), with the thick straight line marking the west coast of Oahu. Terrain elevation of 500 m is shown by the white contour.

Under the trade wind flow, a dynamically induced convergence zone with weak rising motions forms in the lee of Kauai. From morning toward afternoon, the solar heating warms the island, and a sea breeze develops with increased cloudiness over the leeside land. Warm air moving downstream from the island (warm advection by the trade winds) increases the air temperature and lowers pressure in the marine boundary layer, enhancing low-level wind convergence and upward motion in the wake, and leading to the formation of the trail cloud band. At night, the island cools by longwave radiation, and cold air moving downstream from the island (the cold advection) induces downward motion in the wake, suppressing cloud formation. In our simulations for summer 2005, the diurnal temperature anomalies reach a maximum of slightly less than 1.0 K at 500 m MSL because, at the surface, the turbulent heat flux restores air temperature toward sea surface

temperature, which does not include the diurnal cycle in the model.

Both observations and numerical simulation suggest that the wake cloud band lee of Kauai is sensitive to the trade wind strength, with cloudiness increasing with the trade wind speed. The dynamically induced leeside circulations under the strong and weak trades are roughly in the same flow regime with the wake. The diurnal cycle of air temperature increases in amplitude over the leeside sea in the strong wind composite in the model. The increased warm advection is the major cause (two-thirds) of the enhanced wind convergence in the wake, while the increased dynamical forcing in response to stronger impinging trades makes a minor but significant contribution (one-third).

The similarities in the wake cloud band and its diurnal cycle between Kauai and Oahu Islands suggest that the thermal wake effect is ubiquitous. A comparison of

Nauru, Niihau, Kauai, Oahu, and Hawaii offers some insights into the roles of mountain height and island size on trail cloud formation. Nauru is flat with maximum elevation 60 m, illustrating that lee trail clouds can form under very weak dynamical forcing. The dynamical forcing of moderately tall islands like Kauai and Oahu creates weak convergence in the lee favorable for trail clouds development. For a tall island like Hawaii (4.2 km in elevation), however, a dynamically induced return flow can develop in the wake and, together with the sea breeze, prevent large diurnal warming over the island from being advected into the wake. As a result, trail clouds do not develop in the cold wake of Hawaii during daytime (Fig. 18c). Regarding island size, the small islands of Nauru (only 21.2 km<sup>2</sup> in area) in the tropical western Pacific (Porch et al. 2006; McFarlane et al. 2005) and Niihau (Figs. 3–5) west of Kauai force strong diurnal variations of lee trail clouds. A large island may not be favorable for trail cloud development if strong sea breezes develop and reverse the prevailing trades. The above comparison of cloud formation among Nauru, Niihau, Kauai, Oahu, and Hawaii leads to the following hypothesis: daytime trail clouds develop in Kauai-type warm wakes without a reverse flow under moderate-to-weak dynamical forcing by island orography, whereas they do not develop in Hawaii-type wakes with an onshore reverse flow under strong island dynamical forcing. Additional surveys of cloud formation over other tropical and subtropical islands will shed further light on island dynamical versus thermal effects.

*Acknowledgments.* This study is supported by the NOAA PRIDE Program, NASA, and JAMSTEC. The authors wish to thank the NCAR MM5 group for the applications of the MM5–LSM, anonymous reviewers for useful comments, P. Hacker for encouragement, Y.-L. Chen for useful discussions at the early stage of this study, and D. Henderson for editing the text.

#### REFERENCES

- Bauer, M. H., G. J. Mary, I. Vergeiner, and H. Pichler, 2000: Strongly nonlinear flow over and around a three-dimensional mountain as a function of the horizontal aspect ratio. *J. Atmos. Sci.*, **57**, 3971–3991.
- Burk, S. D., T. Haack, L. T. Rogers, and L. J. Wagner, 2003: Island wake dynamics and wake influence on the evaporation duct and radar propagation. *J. Appl. Meteor.*, **42**, 349–367.
- Chen, F., and J. Dudhia, 2001: Coupling an advanced land surface-hydrology model with the Penn State–NCAR MM5 modeling system. Part I: Model implementation and sensitivity. *Mon. Wea. Rev.*, **129**, 569–585.
- Chen, Y.-L., and A. J. Nash, 1994: Diurnal variations of surface airflow and rainfall frequencies on the island of Hawaii. *Mon. Wea. Rev.*, **122**, 34–56.
- Chopra, K. P., 1973: Atmospheric and oceanic flow problems introduced by islands. *Advances in Geophysics*, Vol. 16, Academic Press, 297–421.
- , and L. F. Hubert, 1965: Mesoscale eddies in wake of islands. *J. Atmos. Sci.*, **22**, 652–657.
- Ding, L., and R. L. Street, 2003: Numerical study of the wake structure behind a three-dimensional hill. *J. Atmos. Sci.*, **60**, 1678–1690.
- Dorman, C. E., 1994: Guadalupe Island cloud trail. *Mon. Wea. Rev.*, **122**, 235–242.
- Dudhia, J., 1993: A nonhydrostatic version of the Penn State–NCAR mesoscale model: Validation tests and simulation of an Atlantic cyclone and cold front. *Mon. Wea. Rev.*, **121**, 1493–1513.
- , and M. W. Moncrieff, 1989: A three-dimensional numerical study of an Oklahoma squall line containing right-flank supercells. *J. Atmos. Sci.*, **46**, 3363–3391.
- Foote, D. E., E. L. Hill, S. Nakamura, and F. Stephens, 1972: Soil survey of islands of Kauai, Oahu, Maui, Molokai, and Lanai, State of Hawaii. Soil Conservation Service, U.S. Dept. of Agriculture, in cooperation with the University of Hawaii Agricultural Experiment Station, 115 pp. [Available from Natural Resources Conservation Service, U.S. Dept. of Agriculture, Rm. 4-118, 300 Ala Moana Blvd., Honolulu, HI 96850.]
- Giambelluca, T. W., M. A. Nullet, and T. A. Schroeder, 1986: Rainfall atlas of Hawaii. Department of Land and Natural Resources Rep. R76, State of Hawaii, Honolulu, HI, 267 pp.
- Hafner, J., and S.-P. Xie, 2003: Far-field simulation of the Hawaiian wake: Sea surface temperature and orographic effects. *J. Atmos. Sci.*, **60**, 3021–3032.
- Hong, S.-Y., and H. L. Pan, 1996: Nonlocal boundary layer vertical diffusion in a medium-range forecast model. *Mon. Wea. Rev.*, **124**, 2322–2339.
- Hsie, E.-Y., R. A. Anthes, and D. Keyser, 1984: Numerical simulation of frontogenesis in a moist atmosphere. *J. Atmos. Sci.*, **41**, 2581–2594.
- Hubert, L. F., and A. F. Krueger, 1962: Satellite pictures of mesoscale eddies. *Mon. Wea. Rev.*, **90**, 457–463.
- Lane, T. P., R. D. Sharman, R. G. Frehlich, and J. M. Brown, 2006: Numerical simulation of the wake of Kauai. *J. Appl. Meteor. Climatol.*, **45**, 1313–1331.
- Leopold, L. B., 1949: The interaction of trade wind and sea breeze, Hawaii. *J. Meteor.*, **8**, 533–541.
- Matthews, S., J. M. Hacker, J. Cole, J. Hare, C. N. Long, and R. M. Reynold, 2007: Modification of the atmospheric boundary layer by a small island: Observations from Nauru. *Mon. Wea. Rev.*, **135**, 891–905.
- McFarlane, S. A., C. N. Long, and D. M. Flynn, 2005: Impact of island-induced clouds on surface measurements: Analysis of the ARM Nauru Island effect study data. *J. Appl. Meteor.*, **44**, 1045–1065.
- Nordeen, M. L., P. Minnis, D. R. Doelling, D. Pethick, and L. Nguyen, 2001: Satellite observations of cloud plumes generated by Nauru. *Geophys. Res. Lett.*, **28**, 631–634.
- Porch, W. M., and S. Winiecki, 2003: Tropical western Pacific island cloud trail studies. *Proc. 13th ARM Science Team Meeting*, Broomfield, CO, ARM, 1–3.
- , S. C. Olsen, P. Chylek, M. K. Dubey, B. G. Henderson, and W. Clodius, 2006: Satellite and surface observations of Nauru Island clouds: Differences between El Niño and La Niña periods. *Geophys. Res. Lett.*, **33**, L13804, doi:10.1029/2006GL026339.
- Ramage, C. S., and T. A. Schroeder, 1999: Trade wind rainfall

- atop Mount Waialeale, Kauai. *Mon. Wea. Rev.*, **127**, 2217–2226.
- Reisner, J. M., and P. K. Smolarkiewicz, 1994: Thermally forced low Froude number flow past three-dimensional obstacles. *J. Atmos. Sci.*, **51**, 117–133.
- Rotunno, R., V. Grubisic, and P. K. Smolarkiewicz, 1999: Vorticity and potential vorticity in mountain wakes. *J. Atmos. Sci.*, **56**, 2796–2810.
- Sakamoto, T. T., A. Sumi, S. Emori, T. Nishimura, H. Hasumi, T. Suzuki, and M. Kimoto, 2004: Far-reaching effects of the Hawaiian Islands in the CCSR/NIES/FRCGC high-resolution climate model. *Geophys. Res. Lett.*, **31**, L17212, doi:10.1029/2004GL020907.
- Sasaki, H., and M. Nonaka, 2006: Far-reaching Hawaiian Lee Countercurrent driven by wind-stress curl induced by warm SST band along the current. *Geophys. Res. Lett.*, **33**, L13602, doi:10.1029/2006GL026540.
- Sato, H. H., W. Ikeda, R. Paeth, R. Smythe, and M. Takehiro Jr., 1973: Soil survey of the island of Hawaii, state of Hawaii. Soil Conservation Service, U.S. Dept. of Agriculture, in cooperation with the University of Hawaii Agricultural Experiment Station, 232 pp. [Available from Natural Resources Conservation Service, U.S. Dept. of Agriculture, Room 4-118, 300 Ala Moana Blvd., Honolulu, HI 96850.]
- Schär, C., and R. B. Smith, 1993: Shallow-water flow past isolated topography. Part I: Vorticity production and wake formation. *J. Atmos. Sci.*, **50**, 1373–1400.
- , and D. R. Durran, 1997: Vortex formation and vortex shedding in continuously stratified flows past isolated topography. *J. Atmos. Sci.*, **54**, 534–554.
- Schroeder, T., 1993: Climate controls. *Prevailing Trade Winds*, M. Sanderson, Ed., University of Hawaii Press, 12–36.
- Scorer, R., 1986: *Cloud Investigations by Satellite*. Ellis Horwood, 300 pp.
- Smith, R. B., 1989: Hydrostatic airflow over mountains. *Advances in Geophysics*, Vol. 31, Academic Press, 1–41.
- , and V. Grubišić, 1993: Aerial observation of Hawaii's wake. *J. Atmos. Sci.*, **50**, 3728–3750.
- , A. C. Gleason, P. A. Gluhosky, and V. Grubišić, 1997: The wake of St. Vincent. *J. Atmos. Sci.*, **54**, 606–623.
- Smolarkiewicz, P. K., and R. Rotunno, 1989: Low Froude number flow past three-dimensional obstacles. Part I: Baroclinically generated lee vortices. *J. Atmos. Sci.*, **46**, 1154–1164.
- Sun, W.-Y., and J.-D. Chern, 1993: Diurnal variation of lee vortices in Taiwan and the surrounding area. *J. Atmos. Sci.*, **50**, 3404–3430.
- , and —, 1994: Numerical experiments of vortices in the wake of large idealized mountains. *J. Atmos. Sci.*, **51**, 191–209.
- USGS, 1986: Land use/land cover digital data from 1:250 000 and 1:100 000-scale maps. Data user guide 4, U.S. Geological Survey, Reston, VA, 35 pp.
- Xie, S.-P., W. T. Liu, Q. Liu, and M. Nonaka, 2001: Far-reaching effects of the Hawaiian Islands on the Pacific Ocean–Atmosphere. *Science*, **292**, 2057–2060.
- Yang, Y., and Y.-L. Chen, 2003: Circulations and rainfall on the leeward side of the island of Hawaii during HaRP. *Mon. Wea. Rev.*, **131**, 2525–2542.
- , and —, 2008: Effects of terrain heights and sizes on island-scale circulations and rainfall. *Mon. Wea. Rev.*, **136**, 120–146.
- , —, and F. M. Fujioka, 2005: Numerical simulations of the island induced circulations for the island of Hawaii during HaRP. *Mon. Wea. Rev.*, **133**, 3693–3713.
- Young, G. S., and J. Zawislak, 2006: An observational study of vortex spacing in island wake vortex streets. *Mon. Wea. Rev.*, **134**, 2285–2294.
- Zhang, Y., Y.-L. Chen, S.-Y. Hong, K. Kodama, and H.-M. H. Juang, 2005: Validation of the coupled NCEP mesoscale spectral model and an advanced land surface model over the Hawaiian Islands. Part I: Summer trade wind conditions and a heavy rainfall event. *Wea. Forecasting*, **20**, 847–872.